Validity of the semi-infinite tumor model in diffuse reflectance spectroscopy for epithelial cancer diagnosis: a Monte Carlo study

Caigang Zhu and Quan Liu*

Division of Bioengineering, School of Chemical and Biomedical Engineering, Nanyang Technological University, Singapore 637457, Singapore
**quanliu@ntu.edu.sg*

Abstract: The accurate understanding of optical properties of human tissues plays an important role in the optical diagnosis of early epithelial cancer. Many inverse models used to determine the optical properties of a tumor have assumed that the tumor was semi-infinite, which infers infinite width and length but finite thickness. However, this simplified assumption could lead to large errors for small tumor, especially at the early stages. We used a modified Monte Carlo code, which is able to simulate light transport in a layered tissue model with buried tumor-like targets, to investigate the validity of the semi-infinite tumor assumption in two common epithelial tissue models: a squamous cell carcinoma (SCC) tissue model and a basal cell carcinoma (BCC) tissue model. The SCC tissue model consisted of three layers, i.e. the top epithelium, the middle tumor and the bottom stroma. The BCC tissue model also consisted of three layers, i.e. the top epidermis, the middle tumor and the bottom dermis. Diffuse reflectance was simulated for two common fiber-optic probes. In one probe, both source and detector fibers were perpendicular to the tissue surface; while in the other, both fibers were tilted at 45 degrees relative to the normal axis of the tissue surface. It was demonstrated that the validity of the semi-infinite tumor model depends on both the fiber-optic probe configuration and the tumor dimensions. Two look-up tables, which relate the validity of the semi-infinite tumor model to the tumor width in terms of the source-detector separation, were derived to guide the selection of appropriate tumor models and fiber optic probe configuration for the optical diagnosis of early epithelial cancers.

OCIS codes: (170.3660) Light propagation in tissues; (170.6510) Spectroscopy, tissue diagnostics; (060.2310) Fiber optics; (170.4580) Optical diagnostics for medicine.

References and links

1. American Cancer Society, *Cancer Facts and Figs. 2010* (American Cancer Society, Atlanta, 2010).
2. D. Arifler, R. A. Schwarz, S. K. Chang, and R. Richards-Kortum, "Reflectance spectroscopy for diagnosis of epithelial precancer: model-based analysis of fiber-optic probe designs to resolve spectral information from epithelium and stroma," Appl. Opt. **44**(20), 4291–4305 (2005).
3. D. Arifler, C. MacAulay, M. Follen, and R. Richards-Kortum, "Spatially resolved reflectance spectroscopy for diagnosis of cervical precancer: Monte Carlo modeling and comparison to clinical measurements," J. Biomed. Opt. **11**(6), 064027 (2006).
4. S. K. Chang, M. Y. Dawood, G. Staerkel, U. Utzinger, E. N. Atkinson, R. R. Richards-Kortum, and M. Follen, "Fluorescence spectroscopy for cervical precancer detection: Is there variance across the menstrual cycle?" J. Biomed. Opt. **7**(4), 595–602 (2002).
5. I. Pavlova, C. R. Weber, R. A. Schwarz, M. Williams, A. El-Naggar, A. Gillenwater, and R. Richards-Kortum, "Monte Carlo model to describe depth selective fluorescence spectra of epithelial tissue: applications for diagnosis of oral precancer," J. Biomed. Opt. **13**(6), 064012 (2008).
6. M. C. Skala, G. M. Palmer, K. M. Vrotsos, A. Gendron-Fitzpatrick, and N. Ramanujam, "Comparison of a physical model and principal component analysis for the diagnosis of epithelial neoplasias in vivo using diffuse reflectance spectroscopy," Opt. Express **15**(12), 7863–7875 (2007).

#150891 - $15.00 USD Received 15 Jul 2011; revised 21 Aug 2011; accepted 21 Aug 2011; published 25 Aug 2011

7. U. Utzinger, D. L. Heintzelman, A. Mahadevan-Jansen, A. Malpica, M. Follen, and R. Richards-Kortum, "Near-infrared Raman spectroscopy for in vivo detection of cervical precancers," Appl. Spectrosc. **55**(8), 955–959 (2001).
8. Q. Liu and N. Ramanujam, "Sequential estimation of optical properties of a two-layered epithelial tissue model from depth-resolved ultraviolet-visible diffuse reflectance spectra," Appl. Opt. **45**(19), 4776–4790 (2006).
9. E. Drakaki, E. Kaselouris, M. Makropoulou, A. A. Serafetinides, A. Tsenga, A. J. Stratigos, A. D. Katsambas, and C. Antoniou, "Laser-induced fluorescence and reflectance spectroscopy for the discrimination of basal cell carcinoma from the surrounding normal skin tissue," Skin Pharmacol. Physiol. **22**(3), 158–165 (2009).
10. R. M. P. Doornbos, R. Lang, M. C. Aalders, F. W. Cross, and H. J. C. M. Sterenborg, "The determination of in vivo human tissue optical properties and absolute chromophore concentrations using spatially resolved steady-state diffuse reflectance spectroscopy," Phys. Med. Biol. **44**(4), 967–981 (1999).
11. S. Merritt, F. Bevilacqua, A. J. Durkin, D. J. Cuccia, R. Lanning, B. J. Tromberg, G. Gulsen, H. Yu, J. Wang, and O. Nalcioglu, "Coregistration of diffuse optical spectroscopy and magnetic resonance imaging in a rat tumor model," Appl. Opt. **42**(16), 2951–2959 (2003).
12. G. M. Palmer, C. F. Zhu, T. M. Breslin, F. S. Xu, K. W. Gilchrist, and N. Ramanujam, "Monte Carlo-based inverse model for calculating tissue optical properties. Part II: Application to breast cancer diagnosis," Appl. Opt. **45**(5), 1072–1078 (2006).
13. W. Verkruysse, R. Zhang, B. Choi, G. Lucassen, L. O. Svaasand, and J. S. Nelson, "A library based fitting method for visual reflectance spectroscopy of human skin," Phys. Med. Biol. **50**(1), 57–70 (2005).
14. G. Zonios, L. T. Perelman, V. M. Backman, R. Manoharan, M. Fitzmaurice, J. Van Dam, and M. S. Feld, "Diffuse reflectance spectroscopy of human adenomatous colon polyps in vivo," Appl. Opt. **38**(31), 6628–6637 (1999).
15. B. C. Wilson and G. Adam, "A Monte Carlo model for the absorption and flux distributions of light in tissue," Med. Phys. **10**(6), 824–830 (1983).
16. Q. Liu and N. Ramanujam, "Scaling method for fast Monte Carlo simulation of diffuse reflectance spectra from multilayered turbid media," J. Opt. Soc. Am. A **24**(4), 1011–1025 (2007).
17. S. T. Flock, M. S. Patterson, B. C. Wilson, and D. R. Wyman, "Monte-Carlo modeling of light-propagation in highly scattering tissues. 1. Model predictions and comparison with diffusion-theory," IEEE Trans. Bio-Med. Eng. **36**(12), 1162–1168 (1989).
18. C. K. Hayakawa, J. Spanier, F. Bevilacqua, A. K. Dunn, J. S. You, B. J. Tromberg, and V. Venugopalan, "Perturbation Monte Carlo methods to solve inverse photon migration problems in heterogeneous tissues," Opt. Lett. **26**(17), 1335–1337 (2001).
19. G. M. Palmer and N. Ramanujam, "Monte Carlo-based inverse model for calculating tissue optical properties. Part I: Theory and validation on synthetic phantoms," Appl. Opt. **45**(5), 1062–1071 (2006).
20. C. M. Gardner and A. J. Welch, "Monte Carlo simulation of light transport in tissue: unscattered absorption events," Appl. Opt. **33**(13), 2743–2745 (1994).
21. L. H. Wang, S. L. Jacques, and L. Q. Zheng, "MCML--Monte Carlo modeling of light transport in multi-layered tissues," Comput. Methods Programs Biomed. **47**(2), 131–146 (1995).
22. Q. Liu, C. F. Zhu, and N. Ramanujam, "Experimental validation of Monte Carlo modeling of fluorescence in tissues in the UV-visible spectrum," J. Biomed. Opt. **8**(2), 223–236 (2003).
23. C. Zhu and Q. Liu, "Validity of the semi-infinite tumor model in tissue optics: a Monte Carlo study," in *2010 Photonics Global Conference (PGC)* (IEEE, 2010), pp. 1–4
24. B. L. Allen-Hoffmann, S. J. Schlosser, C. A. R. Ivarie, C. A. Sattler, L. F. Meisner, and S. L. O'Connor, "Normal growth and differentiation in a spontaneously immortalized near-diploid human keratinocyte cell line, NIKS," J. Invest. Dermatol. **114**(3), 444–455 (2000).
25. L. Quan and N. Ramanujam, "Relationship between depth of a target in a turbid medium and fluorescence measured by a variable-aperture method," Opt. Lett. **27**(2), 104–106 (2002).
26. C. Kortun, Y. R. Hijazi, and D. Arifler, "Combined Monte Carlo and finite-difference time-domain modeling for biophotonic analysis: implications on reflectance-based diagnosis of epithelial precancer," J. Biomed. Opt. **13**(3), 034014 (2008).
27. S. K. Chang, D. Arifler, R. Drezek, M. Follen, and R. Richards-Kortum, "Analytical model to describe fluorescence spectra of normal and preneoplastic epithelial tissue: comparison with Monte Carlo simulations and clinical measurements," J. Biomed. Opt. **9**(3), 511–522 (2004).
28. V. Kumar, A. K. Abbas, N. Fausto, and J. Aster, eds., *Robbins and Cotran Pathologic Basis of Disease,* 8th ed. (Saunders, 2009), pp. 1180–1181.
29. J. Choi, J. Choo, H. Chung, D. G. Gweon, J. Park, H. J. Kim, S. Park, and C. H. Oh, "Direct observation of spectral differences between normal and basal cell carcinoma (BCC) tissues using confocal Raman microscopy," Biopolymers **77**(5), 264–272 (2005).
30. Y. Lee and K. Hwang, "Skin thickness of Korean adults," Surg. Radiol. Anat. **24**(3-4), 183–189 (2002).
31. E. Salomatina, B. Jiang, J. Novak, and A. N. Yaroslavsky, "Optical properties of normal and cancerous human skin in the visible and near-infrared spectral range," J. Biomed. Opt. **11**(6), 064026 (2006).
32. Q. Liu and N. Ramanujam, "Experimental proof of the feasibility of using an angled fiber-optic probe for depth-sensitive fluorescence spectroscopy of turbid media," Opt. Lett. **29**(17), 2034–2036 (2004).
33. T. J. Pfefer, A. Agrawal, and R. A. Drezek, "Oblique-incidence illumination and collection for depth-selective fluorescence spectroscopy," J. Biomed. Opt. **10**(4), 044016 (2005).
34. A. M. J. Wang, J. E. Bender, J. Pfefer, U. Utzinger, and R. A. Drezek, "Depth-sensitive reflectance measurements using obliquely oriented fiber probes," J. Biomed. Opt. **10**(4), 044017 (2005).

#150891 - $15.00 USD Received 15 Jul 2011; revised 21 Aug 2011; accepted 21 Aug 2011; published 25 Aug 2011

35. D. C. Walker, B. H. Brown, A. D. Blackett, J. Tidy, and R. H. Smallwood, "A study of the morphological parameters of cervical squamous epithelium," Physiol. Meas. **24**(1), 121–135 (2003).
36. R. Drezek, K. Sokolov, U. Utzinger, I. Boiko, A. Malpica, M. Follen, and R. Richards-Kortum, "Understanding the contributions of NADH and collagen to cervical tissue fluorescence spectra: modeling, measurements, and implications," J. Biomed. Opt. **6**(4), 385–396 (2001).
37. J. Qu, C. Macaulay, S. Lam, and B. Palcic, "Optical properties of normal and carcinomatous bronchial tissue," Appl. Opt. **33**(31), 7397–7405 (1994).
38. S. Prestin, C. Betz, and M. Kraft, "Measurement of epithelial thickness within the oral cavity using optical coherence tomography (OCT)," Proc. SPIE **7548**, 75482F, 75482F-9 (2010).
39. R. Sharma, "Gadolinium toxicity: epidermis thickness measurement by magnetic resonance imaging at 500 MHz," Skin Res. Technol. **16**(3), 339–353 (2010).

1. Introduction

Epithelial tissues cover many important organs including the cervix, skin and oral cavity. Over half of human cancers arise in the epithelium and more than two million patients with non-melanoma cancers in the epithelial tissue are identified each year in the US alone [1]. Since the detection of epithelial cancer at an early stage could significantly reduce its morbidity and mortality, the early detection of epithelial cancer has been a hot research area in the past decades [2–8].

Ultraviolet-visible diffuse reflectance spectroscopy has been explored for the detection of early epithelial cancers for years [8–14]. In this technique, the Monte Carlo method has been considered as a gold standard tool to study light transport in tissues since 1980s [15] for providing guidance on the design of optical setups for tissue measurements [16]. Compared to analytical models such as diffusion theory, the Monte Carlo method can be used in a much broader range of optical properties and measurement geometry. Hence it is frequently used to validate the results from analytical models [17]. Moreover, one unique advantage of the Monte Carlo method is its ability to simulate light fluence rate distribution inside a complex tissue model. Because Monte Carlo simulations are generally time consuming, a variety of methods have been developed to accelerate the simulations so that this method could be used to solve inverse problems, for example, to determine the optical properties of a tissue sample for optical diagnosis [8,18,19].

The most common tissue model used in three-dimensional Monte Carlo simulations assumes a layered structure, in which the tissue consists of one or more layers with homogeneous optical properties within each layer [20,21]. Every tissue layer is assumed to be semi-infinite, which infers infinite width and length, but finite thickness. While this semi-infinite model works fine for large tumors, it may result in significant deviation from actual measurements when applied on small tumors at early stage. This would consequently cause inaccurate diagnosis.

The focus of this study is to investigate the validity of the semi-infinite tumor model in two commonly seen epithelial cancers, i.e. squamous cell carcinoma (SCC) and basal cell carcinoma (BCC). Two fiber-optic probe configurations, including one with fibers perpendicular to the tissue surface and the other with tilted fibers, were examined. The dependence of diffuse reflectance on the variation of the tumor width, ranging from zero (corresponding to the case of no tumor) to infinity (corresponding to a semi-infinite tumor), was evaluated in both SCC and BCC models. Moreover, the effects of the tumor thickness, the source-detector separation, and the tilt angles of source and detector fibers on the validity of the semi-infinite tumor model were studied. Two look-up tables, which relate the validity of the semi-infinite tumor model to the tumor width in terms of the source-detector separation, were given to guide the tumor model selection in diffuse reflectance spectroscopy. Finally, the effects of the top layer's thickness and the emission wavelength on the simulation results were discussed.

#150891 - $15.00 USD Received 15 Jul 2011; revised 21 Aug 2011; accepted 21 Aug 2011; published 25 Aug 2011

2. Materials and methods

2.1 The Monte Carlo code and probe configurations

A Monte Carlo code previously developed by our group [22], which was based on a public-domain Monte Carlo code [21], was modified to simulate light transport in a layered tissue model with a buried tumor-like target. An infinite-length cuboid target with specified thickness, width and position was used to mimic an early tumor. The details and validation of the code have been described elsewhere [23].

Two commonly used probe configurations were examined, as shown in Fig. 1. In Fig. 1(a), both fibers were perpendicular to the tissue surface thus the tilt angles of both fibers relative to the normal axis of the tissue surface were 0 degree. The center-to-center distance between the source and detector fibers (S-D), was varied from 200 μm to 800 μm with an increment of 200 μm. In Fig. 1 (b), the tilt angles of both fibers relative to the normal axis of the tissue surface were 45 degrees and the S-D was varied from 400 μm to 600 μm, and then to 800 μm. The diameters of all fibers were 200 μm and the numerical aperture (NA) was 0.22. The refractive indices of all the fibers were set to 1.47. Ten million photons were launched in all simulations.

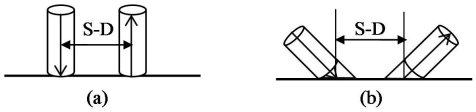

Fig. 1. Probe configurations with tilt angles of both fibers at (a) 0 degree and (b) 45 degrees, relative to the normal axis of the tissue surface. The two cylinders in both sets represent the source and detector fibers and the arrows indicate the direction of light propagation. The acronym S-D represents the center-to-center distance between source and detector fibers.

2.2 Squamous cell carcinoma (SCC) tissue model

An epithelial tissue is typically composed of two layers, the epithelium on the top and the stroma at the bottom. The basement membrane separates the two layers. In the development of an SCC, the tumor usually originates from the basement membrane of the epithelium [24]. The tumor first proliferates upward; after the entire epithelium is occupied, the tumor will invade into the basement membrane towards the stroma. Therefore an epithelial tissue model with SCC used in the literature [25]consists of three layers, i.e. the epithelium on the top, the tumor in the middle and the stroma at the bottom. Each of these three layers was assumed to be semi-infinite in which the thickness is finite while the width and length are infinite.

We studied two SCC models, as shown in Fig. 2, with (a) a semi-infinite and (b) a finite-width tumor in our simulation. The epithelial thickness was set to be 300 μm and the thickness of the stroma was set to be 2050 μm to mimic a thick tissue. The optical properties of each layer were obtained from the literature [26] and listed in Table 1. A refractive index of 1.4 was used in all tissue layers [27]. The anisotropy factors for the epithelium and the tumor were set to 0.97 and an anisotropy factor of 0.8 was used for the stroma [27]. In the semi-infinite tumor model [Fig. 2 (a)], the epithelium, tumor and stroma were assumed to have infinite width and length. For the finite-width tumor model [Fig. 2 (b)], an infinite-length tumor with finite thickness and width, was introduced into the epithelium. In all simulations, the central axis of the tissue model bisects the source and detector fibers in Fig. 1 and the tumors in Fig. 2 on the cross section view.

Totally two sets of simulations were performed on every SCC tissue models, one for each probe configuration. In each set, the thickness of the tumor was varied from 100 μm to 200 μm to investigate the effect of the tumor thickness. For each thickness, the width of the tumor as in Fig. 2(b) was varied from zero to a large value with uneven increments to find the minimum width of the tumor required for the validity of the semi-infinite tumor model as in Fig. 2(a). A threshold value of the tumor width was determined for all tumor thicknesses to

#150891 - $15.00 USD Received 15 Jul 2011; revised 21 Aug 2011; accepted 21 Aug 2011; published 25 Aug 2011

guide the selection of the semi-infinite tumor or finite-width tumor in the SCC tissue model, based on the tumor size.

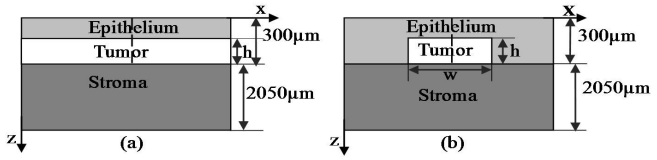

Fig. 2. Cross section schematics of the squamous cell carcinoma (SCC) tissue models (a) with a semi-infinite tumor and (b) with a finite-width tumor. The central dashed lines in both (a) and (b) give the central axes of the tissue model used in the simulations, which bisects the source and detector fibers in Fig. 1 and the tumor in Fig. 2 on the cross section view. In the finite-width model, the tumor has a specified finite thickness (h) and width (w).

Table 1. Optical properties of the SCC tissue model at 500nm [26]

Tissue	Optical properties[a]		
	$\mu_a(cm^{-1})$	$\mu_s(cm^{-1})$	g
Epithelium	2.0	35.6	0.97
Tumor	2.0	106.8	0.97
Stroma	9.1	223.7	0.8

[a]Note: μ_a, absorption coefficient; μ_s, scattering coefficient; g, anisotropy.

2.3 Basal cell carcinoma (BCC) tissue model

Basal cell carcinoma is a common form in non-melanoma cancer of skin, which consists of a BCC tumor sandwiched in between the superficial epidermis and the underlying dermis. The tumor in basal cell carcinoma originates from the basal layer of the epidermis, frequently grows downward deeply into the dermis [28,29].

Two BCC models were examined in our simulations, as shown in Fig. 3, with (a) semi-infinite tumor and (b) a finite-width tumor. The width and length of the epidermis were assumed to be infinitely large, while the epidermal thickness was set to be 80 μm and the thickness of the dermis was set to be 2000 μm to mimic a thick skin tissue. These values are the typical skin thickness for BCC frequently occurs on the neck and back [30], although the epidermal thickness could vary with organ sites. In addition, the absorption coefficient, scattering coefficient and anisotropy used in our simulation were taken from the literature and listed in Table 2 [31]. A refractive index of 1.4 and an anisotropy factor of 0.8 were used in all the three layers [31]. In the BCC model with a semi-infinite tumor [Fig. 3(a)], the tumor has an infinite width. In the BCC tissue model with a finite-width tumor, an infinite-length tumor with finite thickness and width was introduced into the dermis [Fig. 3 (b)]. Similar to the SCC models, the central axis of the tissue model bisects the source and detector fibers as in Fig. 1 and the tumors in Fig. 3 on the cross section view.

The BCC tissue model simulations were performed on fiber probe configurations with tilt angles of 0 degree and 45 degrees. The thickness of the tumor was varied from 200 μm to

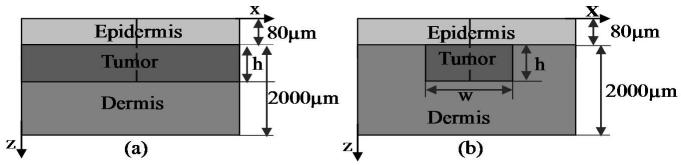

Fig. 3. Cross section of the basal cell carcinoma (BCC) tissue model (a) with a semi-infinite tumor and (b) with a finite-width tumor. The central dashed lines in both (a) and (b) represent the central axes of the coordinate systems used in the simulations, bisects the source and detector fibers as in Fig. 1 and the tumors in Fig. 3 on the cross section view. In finite-width tumor model, the tumor has a specified finite thickness (h) and width (w).

#150891 - $15.00 USD Received 15 Jul 2011; revised 21 Aug 2011; accepted 21 Aug 2011; published 25 Aug 2011

Table 2. Optical properties of BCC tissue model at 500nm [31]

Tissue	Optical properties[a]		
	$\mu_a(cm^{-1})$	$\mu_s(cm^{-1})$	g
Epidermis	7.0	350	0.8
Tumor	3.1	160	0.8
Dermis	3.5	250	0.8

[a]Note: μ_a, absorption coefficient; μ_s, scattering coefficient; g, anisotropy.

400μm for each fiber probe configuration. The tumor width was increased from zero [finite-width tumor in Fig. 3(b)] to infinity [semi-infinite tumor in Fig. 3(b)] with uneven increments for thicknesses of 200 μm and 400μm, respectively, to determine the minimum threshold of the tumor width for the validity of the semi-infinite tumor model.

3. Results

In the following results for both SCC and BCC models, the diffuse reflectance values simulated for each fiber configuration and tumor model were plotted as a function of the tumor width in terms of the source-detector separation (S-D). The diffuse reflectance corresponding to the finite tumor widths were compared to the last data point in each curve that corresponds to the semi-infinite tumor model by performing the unpaired two-sample t test. For those data points corresponding to small tumor widths that are likely to be different from the last data point, five repeated simulations have been performed to estimate the means and standard deviations for the construction of error bars. Those circled data points in Figs. 4–7 indicate statistically significant differences from the last data point with a p-value smaller than 0.05. The threshold value is defined as the smallest tumor width at which the finite tumor model is statistically equivalent to the semi-infinite tumor model in terms of simulated diffuse reflectance.

3.1 Results for the SCC tissue model

Simulated diffuse reflectance values as a function of the tumor width for the SCC tissue model are shown in Figs. 4 and 5, which correspond to tilt angles of 0 degree and 45 degrees, respectively.

Figure 4 shows that there are no significant differences in simulated diffuse reflectance values between the SCC tissue models with a finite-width tumor at different widths and that with a semi-infinite tumor for the probe configuration with zero-degree tilt angle. The diffuse reflectance value decreases with the increment of S-D. Interestingly, the diffuse reflectance changes only minimally when the tumor thickness increases from 100 μm to 200 μm. This should be mainly due to the fact that the absorption coefficients of the epithelium and the tumor were equal. Moreover, the small thickness and the high anisotropy factor of the epithelium minimized the effect of different scattering coefficients on detected diffuse reflectance.

In contrast, Fig. 5 reveals that the probe configuration at 45-degree tilt angle in the SCC tissue model shows significant differences in diffuse reflectance between the models with a semi-infinite tumor and those with a finite-width tumor for tumor widths smaller than a threshold value as highlighted by circled data points. The threshold values of the tumor width for S-D at 400 μm, 600 μm and 800 μm were around 0.75, 1 and 1 time of S-D when the tumor thickness was 100 μm. These threshold values did not change when the tumor thickness was increased to 200 μm.

3.2 Results for the BCC tissue model

Simulated diffuse reflectance as a function of the tumor width for the BCC tissue model are shown in Figs. 6 and 7, which correspond to tilt angles of 0 degree and 45 degrees, respectively.

#150891 - $15.00 USD Received 15 Jul 2011; revised 21 Aug 2011; accepted 21 Aug 2011; published 25 Aug 2011

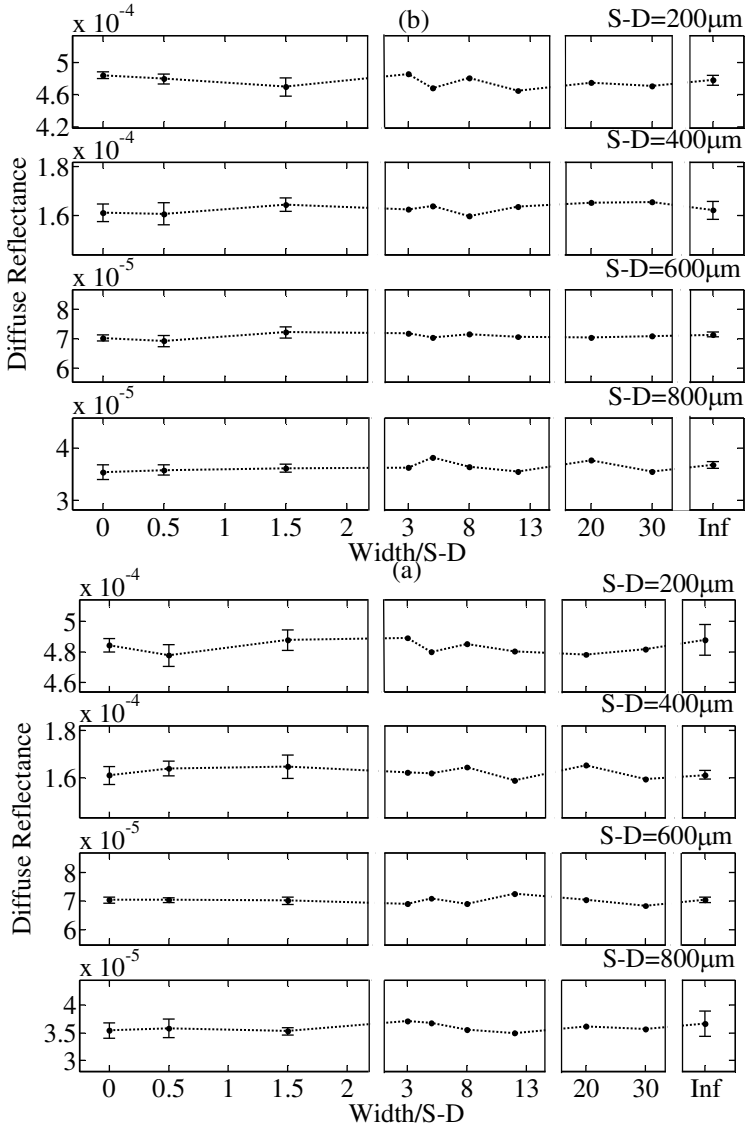

Fig. 4. Simulated diffuse reflectance as a function of the tumor width in terms of the source-detector separation (S-D) when the tumor thickness was fixed at (a) 100 μm and (b) 200 μm in a squamous cell carcinoma (SCC) tissue model. The tilt angles of all fibers were fixed at 0 degree and the S-D was varied from 200 μm to 800 μm with an increment of 200 μm. Each curve is divided into four segments according to the increment of the tumor width on the horizontal axis. The error bars at initial data points and the last data point represent the standard deviation of the data. The label "Inf" on the horizontal axis stands for "Infinity."

Different from the results for the SCC tissue model, the simulated diffuse reflectance changes significantly with the tumor width in the BCC tissue model as shown in Fig. 6 even when the tilt angles of source and detector fibers are zero degree. Consequently, a significant difference can be observed between the BCC tissue models with finite-width tumors and that with a semi-infinite tumor when the tumor width was smaller than a threshold value as highlighted by circled data points in Fig. 6. The threshold values of the tumor width for the S-D of 200 μm, 400 μm, and 600 μm and 800 μm were around 3, 2, 1.25 and 1.25 times of S-D when the thickness of tumor was 200 μm. The threshold values changed to around 2, 1.75, 1.5 and 1.25 times of S-D when the tumor thickness was 400 μm.

#150891 - $15.00 USD Received 15 Jul 2011; revised 21 Aug 2011; accepted 21 Aug 2011; published 25 Aug 2011

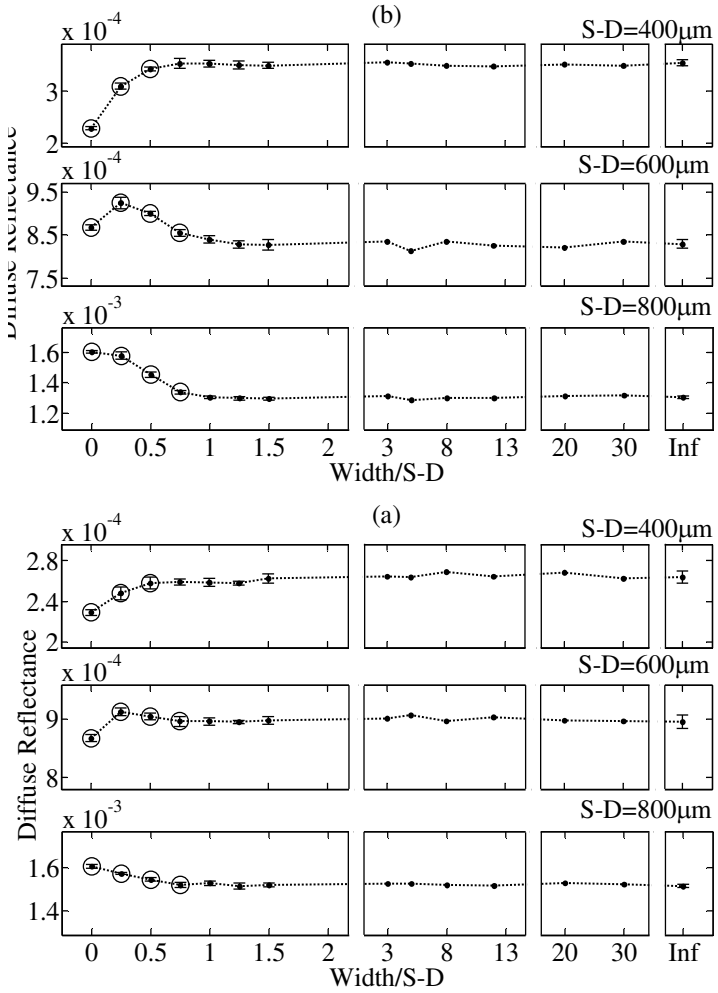

Fig. 5. Simulated diffuse reflectance as a function of the tumor width in terms of the source-detector separation (S-D) when the tumor thickness was fixed at (a) 100 μm and (b) 200 μm in a squamous cell carcinoma (SCC) tissue model. The tilt angles of all fibers were fixed at 45 degrees and the S-D was varied from 400 μm to 800 μm with an increment of 200 μm. Each curve is divided into four segments according to the increment of the tumor width on the horizontal axis. The error bars at initial data points and the last data point represent the standard deviation of the data. Among these data points, the circled ones are statistically different from that for the SCC tissue model with a semi-infinite tumor, which corresponds to the last data point in each subplot. The label "Inf" on the horizontal axis stands for "Infinity."

When the tilt angles of source and detector fibers were 45 degrees, both the detected diffuse reflectance and the threshold values changed as shown in Fig. 7 compared to the case of zero-degree tilt angles in Fig. 6. The threshold values of the tumor width for the S-D of 400 μm, 600 μm and 800 μm were around 1, 1.75 and 1 times of S-D when the tumor thickness was 200 μm. The threshold values changed to around 1.25, 1 and 1 times of S-D when the tumor thickness was 400μm. Similar to Fig. 6, it appears that the threshold values changed only moderately with the tumor thickness.

Tables 3 and 4 summarize the threshold values for the various tumor thicknesses and probe configurations in the SCC tissue model and the BCC tissue model, respectively. The zero threshold value implies that the SCC tissue models with finite-width tumors are similar (statistical difference with a p-value greater than 0.05) to that with a semi-infinite tumor in

#150891 - $15.00 USD Received 15 Jul 2011; revised 21 Aug 2011; accepted 21 Aug 2011; published 25 Aug 2011

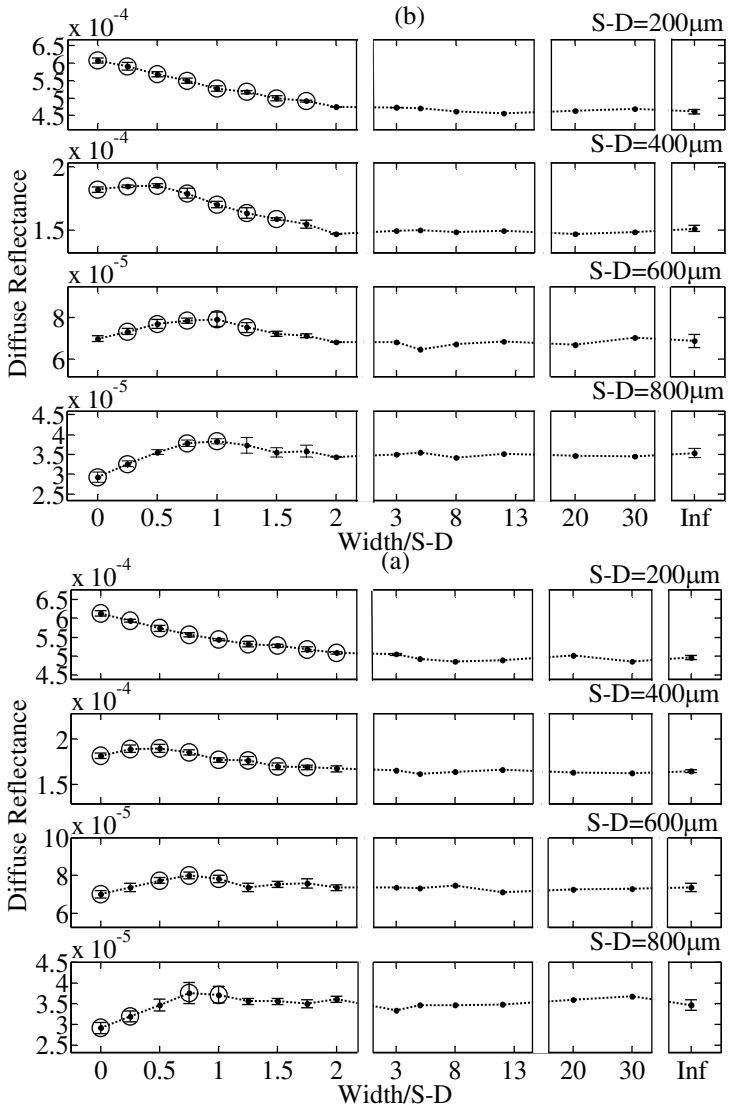

Fig. 6. Simulated diffuse reflectance as a function of the tumor width in terms of the source-detector separation (S-D) when the thickness of tumor was fixed at (a) 200 μm and (b) 400 μm in a basal cell carcinoma (BCC) tissue model. The tilt angles of all fibers were fixed at 0 degree and the S-D was varied from 200 μm to 800 μm with an increment of 200 μm. Each curve is divided into four segments according to the increment of the tumor width on the horizontal axis. The error bars at initial data points and the last data point represent the standard deviation of the data. Among these data points, the circled ones are statistically different from that for the BCC tissue model with a semi-infinite tumor, which corresponds to the last data point in each subplot. The label "Inf" on the horizontal axis stands for "Infinity."

diffuse reflectance for all tumor widths under evaluation. In summary, the variations in the S-D, tumor thickness and tilt angle of source and detector fibers, have an effect on the threshold value of tumor width/S-D for the validity of the semi-infinite tumor model.

#150891 - $15.00 USD Received 15 Jul 2011; revised 21 Aug 2011; accepted 21 Aug 2011; published 25 Aug 2011

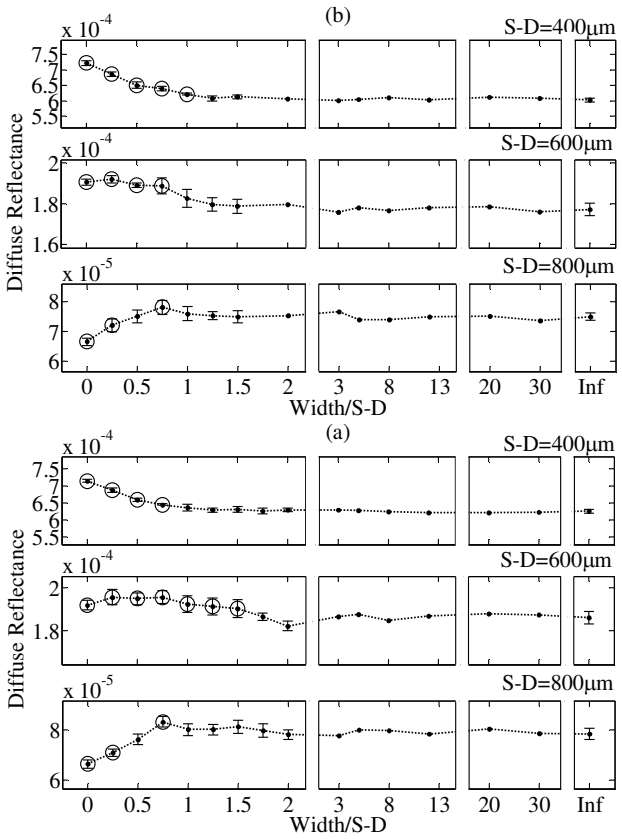

Fig. 7. Simulated diffuse reflectance as a function of the tumor width in terms of the source-detector separation (S-D) when the tumor thickness was fixed at (a) 200 μm and (b) 400 μm in a basal cell carcinoma (BCC) tissue model. The tilt angles of all fibers were fixed at 45 degrees and the S-D was varied from 400 μm to 800 μm with an increment of 200 μm. Each curve is divided into four segments according to the increment of the tumor width on the horizontal axis. The error bars at initial data points and the last data point represent the standard deviation of the data. Among these data points, the circled ones are statistically different from that for the BCC tissue model with a semi-infinite tumor, which corresponds to the last data point in each subplot. The label "Inf" on the horizontal axis stands for "Infinity."

Table 3. Threshold value of tumor width for the valid semi-infinite SCC tumor model

Tumor thickness	100 μm		200 μm	
	Tilt angle[a] (degrees)			
S-D(μm)	*0*	*45*	*0*	*45*
200	0	NA	0	NA
400	0	0.75	0	0.75
600	0	1	0	1
800	0	1	0	1

[a]Note: "NA" stands for "not available."

Table 4. Threshold value of tumor width for the valid semi-infinite BCC tumor model

Tumor thickness	200 μm		400 μm	
	Tilt angle[a] (degrees)			
S-D (μm)	*0*	*45*	*0*	*45*
200	3	NA	2	NA
400	2	1	1.75	1.25
600	1.25	1.75	1.5	1
800	1.25	1	1.25	1

[a]Note: "NA" stands for "not available."

#150891 - $15.00 USD Received 15 Jul 2011; revised 21 Aug 2011; accepted 21 Aug 2011; published 25 Aug 2011

4. Discussion

The validity of the semi-infinite tumor model and diffuse reflectance values in the SCC and BCC tissue model are affected by the variations in S-D, tumor thickness and the tilt angle of source and detector fibers. The trends in the threshold value of tumor width threshold for semi-infinite tumor validity and the diffuse reflectance in the SCC and BCC tissue models can be explained by considering light transport in the tissue models as following.

In the SCC tissue models, the simulated diffuse reflectance values are similar for probe configuration with zero-degree tilt angles (Fig. 4), between the semi-infinite SCC tissue model [Fig. 2(a)] and the finite-width SCC tissue models [Fig. 2(b)] when S-D varies from zero to infinity. This observation can be explained by the fact that photons detected in this probe configuration travel only short paths in the tumor arising from the high anisotropy value of 0.97 of the epithelium and tumor. In contrast, significant differences (p-value smaller than 0.05) are observed for the probe configuration with 45-degree tilt angle as highlighted by circled data points in Fig. 5, in the diffuse reflectance values between the finite-width and semi-infinite SCC tissue models. Tilted fibers allowed more photons primarily traveled in the top layer to be detected compared to the probe configuration with zero-degree tilt angle. Therefore, it can be inferred that the probe configuration with 45-degree tilt angle is much more sensitive to the superficial tumor than that with zero-degree title angle, which agrees with previous publications [8,32–34].

In Fig. 5 where the tilt angles of fibers were 45 degrees, it is observed that the threshold value is lower for smaller SD separations in general, which is due to the fact that the fiber-optic probe with a smaller S-D separation probes the tissue volume in a smaller horizontal range.

The diffuse reflectance simulated for finite-width BCC tissue models in the case of the probe configuration with zero tilt angles are different from that for the semi-infinite BCC tissue model as highlighted by circled data points in Fig. 6. This trend is different from that in the SCC tissue model as in Fig. 4. The reason is that the epidermis has an anisotropy value of 0.8 (in comparison to an anisotropy value of 0.97 in the epithelium of the SCC model) thus photons were likely to propagate towards and travel through the BCC tumor. So the probe configuration with a zero-degree tilt angle was more sensitive to the BCC tumor than to the SCC tumor. In addition, the optical properties of the BCC tumor are different from those of the surrounding dermis.

The threshold values in the BCC tissue model for the probe configuration with 45-degree tilt angle are in general smaller than those for the probe configuration with zero-degree tilt angle as shown in Table 4. This is likely due to the fact that the fiber-optic probe with 45-degree tilt angle examines the tissue volume in a smaller horizontal range than that with zero-degree tilt angle.

In the SCC tumor model, we used a commonly cited value, i.e. 300 μm, for the epithelial thickness. However, the epithelial thickness varies significantly, with a typical range from 200 μm to 500 μm [35]. It should be noted that the change of the epithelial thickness may affect the results in this study and this effect is discussed as following. Assuming that the tumor size is fixed, the tumor depth will increase when the total epithelial thickness is increased because the SCC tumor is located at the bottom of the epithelium. Due to the high anisotropy value in the top layer, the effective mean free path in the top layer for the optical properties in Table 1, defined as $1/[\mu_s(1-g)]$, is about 0.94 cm, which is much larger than 500 μm. Therefore most photons would travel directly through the top layer and spend much longer path in the bottom layer just like when the top layer was 300 μm thick in the SCC model. For this reason, we expect that the trend in simulated diffuse reflectance as a function of the tumor width would be similar to Fig. 4 and 5 when the epithelial thickness changes. However, the exact threshold values will be different.

The threshold value depends on the contribution of the tumor to total diffuse reflectance. Only if the contribution of the tumor to simulated diffuse reflectance is significant, there will be a difference in simulated diffuse reflectance between the finite-width tumor model and the

#150891 - $15.00 USD Received 15 Jul 2011; revised 21 Aug 2011; accepted 21 Aug 2011; published 25 Aug 2011

semi-infinite tumor model. Due to the numerical aperture of the fibers, a light delivery cone and a light acceptance cone will be formed at the end of the source and detector fibers, respectively. The overlapping region of the light cones between the source and detector fibers determines the origination of simulated diffuse reflectance, which will be called the detection region in the following discussion. The tumor volume covered by the detection region relative to the total detection region indicates the contribution of the tumor to simulated diffuse reflectance.

For the probe configuration with a zero degree tilt angle, the contribution of the tumor to simulated reflectance is small since the majority of diffuse reflectance is contributed by the deeper stroma as indicated by the tumor volume covered by the detection region in Fig. 8 (a). The contribution of the tumor will increase when the total thickness is increased from 300 μm to 500 μm because a larger tumor volume will be covered by the detection region. Thus the probe configuration will become more sensitive to the tumor and the threshold value will be likely to increase to a non-zero value. In contrast, the contribution of the tumor will decrease when the total thickness is decreased from 300 μm to 200 μm, thus the probe configuration will be still insensitive to the tumor and the threshold value will be still zero.

For the probe configuration with a 45-degree tilt angle and a small S-D, a large portion of the tumor volume is covered by the detection region, as shown in Fig. 8 (b). As the epithelial thickness is increased, the tumor will gradually move out of the detection region. When the tumor is entirely out of the detection region, simulation diffuse reflectance will be insensitive to the tumor width. Before the tumor is out of the detection region, the threshold value of the tumor width depends on the tumor volume covered by the detection region, whose trend is difficult to predict because both the complex shape of the detection region and the tumor height may influence that. It is noted that the detection region shown in Fig. 8(b) will change with the S-D, which will further complicate the prediction of the trend. Similarly, the threshold values will change when the epithelial thickness is decreased from 300 μm to 200 μm but the exact values are difficult to predict.

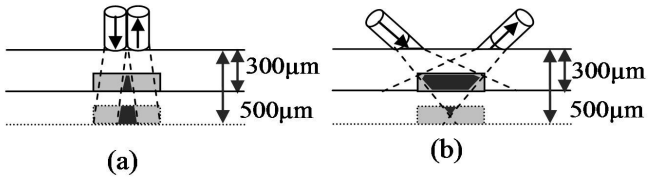

Fig. 8. Schematic of the SCC tumor (light gray color) relative to the detection region (black color) with an increasing epithelial thickness for (a) the probe configuration with a zero-degree tilt angle and (b) the probe configuration with a 45-degree tilt angle. It is assumed that the tumor thickness was fixed to be 100 μm when the epithelial thickness was increased from 300 μm to 500 μm in both (a) and (b).

In the BCC model, the epidermal thickness may affect the results obtained in this study just as in the SCC model. The effective mean free path in the epidermis for the optical properties in Table 2 is around 142 μm. When the epidermal thickness is close to this value or smaller, an incident photon will not change its direction significantly when approaching the tumor thus it is expected that the trends in Fig. 6 and 7 will not change much. However when the epidermal thickness is much larger than 142 μm, the photon will change the direction significantly before it reaches the tumor. In this case, the trends in Fig. 6 and 7 may change dramatically.

Another parameter that usually affects simulation results is the emission wavelength. But we expect that the trends shown in Fig. 4 through Fig. 7 will not change significantly with the emission wavelength. The reason is that the scattering coefficient and the anisotropy value of the tissue models, which are the major factors affecting the amount of photons reaching the tumor change slowly in the visible spectrum in both the SCC tissue model [36] [37]and the BCC tissue model [31].

#150891 - $15.00 USD Received 15 Jul 2011; revised 21 Aug 2011; accepted 21 Aug 2011; published 25 Aug 2011

In the current clinical practice, the size of a skin tumor a clinician can see is usually larger than 1 mm. However, diffuse reflectance spectroscopy as a potential tool for early epithelial cancer diagnosis, could detect skin cancer smaller than 1 mm, which is beyond the capability of the current clinical practice. Moreover, in the epithelial tissues covering many organs such as the cervix or oral cavity, the dysplasia could be smaller than 1 mm at early stages when it is bounded in the epithelium. In these cases, the results from this study will be directly applicable because the S-D values in this study are smaller than 1 mm and the threshold values in Tables 3 and 4 are comparable to the S-D. When the S-D value is much larger than 1 mm, it will be difficult to tell whether the guideline will work without further investigation because the simple interpretation in terms of geometrical optics as shown in Fig. 8 may not work anymore. When the S-D value is very large such as 5 mm, the Monte Carlo code used in this study may not be the best tool to investigate this problem because very few photons would be detected in Monte Carlo simulations at such a large S-D. This would result in unacceptable uncertainty in simulated diffuse reflectance. Other methods such as phantom experiments may be preferred.

Based on the results obtained in this study, it is important to know the tumor width and epithelial thickness (or epidermal thickness) to select an appropriate tumor model. The epithelial thickness and tumor width could be obtained by other imaging modalities, such as optical coherence tomography [38] and magnetic resonance imaging [39], or estimated from clinical examination. Then the following guideline for the validity of the semi-infinite tumor model could be applied in diffuse reflectance spectroscopy, which is based on the threshold values shown in Table 3 and Table 4. For the SCC tissue model with a 300-μm thick epithelium, the semi-infinite SCC model generates statistically equal diffuse reflectance as finite-width SCC models for the probe configuration with a zero-degree tilt angle. This observation implies that this probe configuration is not sensitive to the superficial SCC tumor. For the probe configuration with a 45-degree tilt angle, the minimum threshold values for the semi-infinite tumor model to be valid are 0.75, 1 and 1 time of S-D, respectively. A finite-width tumor model will be more appropriate if the tumor width is smaller than the threshold value. For the BCC tissue model with an 80-μm thick epidermis, both the probe configuration with a zero-degree tilt angle and that with a 45-degree tilt angle are sensitive to the BCC tumor. Table 4 provides the minimum threshold values of the tumor width for the semi-infinite BCC tumor model to be valid. It should be aware that varying the epithelial or epidermal thickness might change the threshold value. When the epithelial or epidermal thickness is different from what have been studied here, the discussion earlier about its effect on the threshold values will help estimate the new threshold value.

In this study, all the finite-width tumors were assumed to be infinite in the length dimension, which does not affect the validity of the guideline. This can be explained by the fact that the dimension of the probed volume in the length dimension, i.e. the direction perpendicular to the plane containing source and detector fibers, is typically comparable to the fiber diameter. Hence, an infinite-length tumor is equivalent to a finite tumor with equal width and thickness and a length comparable to the fiber diameter in terms of light propagation. Since most threshold values are comparable to or larger than the fiber diameter (Tables 3 and 4), the validity of the guideline is still justified for the infinite-length tumor assumption. Nevertheless, future studies are warranted to validate the guideline in tumors with finite size in all dimensions.

5. Conclusion

In conclusion, we have investigated the validity of the semi-infinite tumor model in diffuse reflectance spectroscopy for epithelial cancer diagnosis. Two common epithelial tissue models, including a squamous cell carcinoma tissue model and a basal cell carcinoma tissue model, were examined. It was demonstrate that the validity of the semi-infinite tumor model depends on both fiber-optic probe configuration and tumor dimensions. Two look-up tables were derived to guide the selection of appropriate tumor models and fiber-optic probe configurations in the optical diagnosis of early epithelial cancers. It should be aware that the

#150891 - $15.00 USD Received 15 Jul 2011; revised 21 Aug 2011; accepted 21 Aug 2011; published 25 Aug 2011

threshold values in the look-up tables could change when any key parameter in the tissue model, such as the organ site and tumor stage, or probe specifications, such as the fiber size and numerical aperture, is varied.

Acknowledgments

The authors would like to acknowledge the financial support from Tier 1 grant and Tier 2 grant funded by the Ministry of Education in Singapore (Grant nos. RG47/09 and MOE 2010-T2-1-049).

#150891 - $15.00 USD Received 15 Jul 2011; revised 21 Aug 2011; accepted 21 Aug 2011; published 25 Aug 2011